International Journal of Computational Methods
(2025) 2441012 (15 pages)

DOI: 10.1142/S0219876224410123

Numerical Simulation of Liquid Sloshing in a Spherical Tank by MPS Method

Guohua Pan *, Congyi Huang †, Fengze Xie † and Decheng Wan †,‡

*Ningbo Pilot Station, Ningbo Dagang Pilotage Co., Ltd.
Ningbo, P. R. China

†Computational Marine Hydrodynamic Lab (CMHL)
School of Naval Architecture, Ocean and Civil Engineering
Shanghai Jiao Tong University, Shanghai, P. R. China
‡dcwan@sjtu.edu.cn

Received 31 October 2024
Revised 3 April 2025
Accepted 14 April 2025
Published 24 May 2025

This paper addresses the complex phenomenon of liquid sloshing inside a spherical tank, a subject critical for ensuring structural safety in various applications, notably in aerospace. Utilizing the in-house solver MLParticle-SJTU, based on the Moving Particle Semi-implicit (MPS) method, we simulate liquid sloshing under varying conditions inside a spherical tank. Our focus is on a range of liquid filling rates ($h/R = 0.2$–1.8), where the tank experiences initial excitation and the liquid inside decays freely. The key outcomes include the natural frequencies and damping coefficients at different filling rates. The results indicate a direct correlation between increasing water depth and rising natural frequency, coupled with a decrease in the damping coefficient. This study not only advances our understanding of liquid sloshing dynamics but also contributes valuable insights for designing safer aerospace structures under sloshing conditions.

Keywords: Moving Particle Semi-implicit (MPS) method; liquid sloshing; spherical tank; natural frequency; free decay motion.

1. Introduction

Liquid sloshing is a phenomenon that happens inside a partially loaded tank under external excitation. This phenomenon is produced by the combined effect of surface tension and gravity, and it is a very complex fluid motion phenomenon. There is a free surface, which may have large deformation such as curling and breaking when the sloshing phenomenon is intense, showing a strong nonlinearity. Liquid sloshing is very common in daily life, for example, when a partially loaded liquid cargo ship (such as LNG, LPG, or crude oil ship) encounters wave loads, the movement of

‡Corresponding author.

the tank will stimulate the internal liquid sloshing. When an aircraft is taking off, taxiing, landing, or adjusting attitude in the air, the liquid sloshing will also be triggered inside the oil storage tanks.

The occurrence of liquid sloshing is highly randomized and its potential damage to the structure cannot be ignored. On the one hand, the violent sloshing will generate a great pressure on the bulkhead, leading to deformation or damage of the structure. On the other hand, the liquid sloshing may also stimulate the motion response of the structure, which will cause dynamic instability. Therefore, it is of great significance to accurately simulate and forecast the liquid sloshing phenomena that may occur inside the tank.

There are a lot of researchers who have been working on these liquid sloshing problems. Yang and Peupeot [2014] used Computational Fluid Dynamics (CFD) to simulate the phenomenon of tank sloshing in a spherical liquid tank and gave the equivalent sloshing mass and the equivalent center of mass position through the equations [Yang and Peupeot (2014)]. Gabriele and Jose [2018] simulated the dynamics of a ship with an internal liquid tank sloshing in the time domain by a joint simulation approach. Cao *et al.* [2019] simulated the liquid sloshing phenomenon in a broken ship using the SPH method. Álvaro *et al.* [2021] have studied the equilibrium meniscus and axisymmetric oscillations of a ferrofluid solution in a cylindrical tank subjected to a static nonuniform magnetic field under microgravity conditions for the first time. Mashy *et al.* [2021] used the SPH method to accurately simulate long periods of vigorous oscillatory flow in an arbitrarily shaped partially filled water tank. Chen *et al.* [2022] performed numerical simulations using the fluid–volume method to study the liquid–gas interface on the rotor surface under microgravity conditions and proposed a dimensionless theoretical solution for the profile. Wang *et al.* [2022] performed CFD simulations using a Volume-of-Fluid (VOF) model to analyze the effects of propellant volume fill ratio and acceleration conditions on fluid flow in a blade-type surface tension fuel tank. Yang *et al.* [2022], simulated the intense sloshing flow by the Smoothed Particle Hydrodynamics (SPH) method.

When the external excitation frequency is close to the system's natural frequency, the system will reach the resonance state. At this time, the liquid sloshing is the most violent, the sloshing amplitude is the largest, and the load applied to the structure is also the highest. Therefore, we need to predict the natural frequency with different water depths. In this paper, the freely damped sloshing phenomena inside a tank with different water depths are simulated respectively. The natural frequency and the damping coefficient of the system are calculated.

2. Numerical Method

In this paper, a meshless particle method, the Moving Particle Semi-implicit (MPS) method, is used to simulate the liquid sloshing inside a spherical liquid cabin. The MPS method is a CFD method based on the Lagrangian representation. Different from the traditional mesh-based methods, the MPS method discretizes the

computational domain into a series of particles, which do not have a fixed topological relationship with each other but carry their own physical information, such as displacements, velocities, accelerations, etc., respectively. Compared with the traditional mesh-based methods, the particle method has the advantage that, since there is no mesh in its computation, there will be no mesh distortion or brokenness when simulating the violent flows with free surface large deformation. And the meshless particle method has high quality in tracking the free surface, dealing with the moving boundary and other problems. Therefore, the meshless particle method is very suitable for simulating problems with free surface large deformation characteristics, such as dam–break, water entry and liquid sloshing.

Several works based on the MPS method have been carried out by our group, including algorithm improvement, solver development, and applications For solving the pressure oscillation problems that often occur in the traditional MPS method when calculating the pressure by the Poisson pressure equations, the group has proposed a set of improved MPS algorithms by improving the pressure solving method, the pressure gradient model, and the method of judging the free surface [Zhang and Wan (2014)]. Based on this improved MPS method, our group has developed a meshless particle method solver MLParticle-SJTU, which can be run on the CPU, and multi-CPU parallel computing can also be realized [Zhang (2014)]. In order to make full use of the advantages of the MPS method in simulating violent flows, the group also developed algorithms for coupling the MPS method with other methods, including the MPS-FEM coupling algorithm for simulating fluid–structure coupling phenomena and independently developed the MPSFEM-SJTU solver [Zhang *et al.* (2022b)]. And the MPSDEM coupling algorithm for simulating particle flows and independently developed the MPSDEM-SJTU solver [Xie *et al.* (2021, 2022, 2025)]. However, due to its low efficiency, the MPS method cannot be used in the simulation of large-scale large scale computational applications. Therefore, a high-performance meshless particle solver MPSGPU-SJTU which can run on GPU is developed by our group, and it can improve the computational speed greatly while guaranteeing the precision and accuracy of the original particle solver [Chen and Wan (2019a)]. In previously published papers, the numerical method of the MPS method has been introduced in detail [Tang *et al.* (2016); Huang *et al.* (2022)]. Therefore, in this paper, the MPS method will be introduced simply in the following part.

2.1. *Governing equations*

The governing equations for the MPS method are shown in the following equations:

$$\frac{1}{\rho}\frac{D\rho}{Dt} = -\nabla \cdot \boldsymbol{V} = 0, \tag{1}$$

$$\frac{D\boldsymbol{V}}{Dt} = -\frac{1}{\rho}\nabla p + v\nabla^2 \boldsymbol{V} + \boldsymbol{g}, \tag{2}$$

where ρ is the fluid density, $\boldsymbol{V}$ is the velocity vector, p is the pressure, v is kinematic viscosity, $\boldsymbol{g}$ is gravitational acceleration vector and t indicates time.

2.1.1. *Particle interaction models*

In MPS, particles interact with each other through a kernel function. The kernel function used in this paper is given in Eqs. (3a) and (3b).

$$W(r) = \frac{r_e}{0.85r + 0.15r_e} - 1, \quad 0 \le r < r_e, \tag{3a}$$

$$W(r) = 0, \quad r_e \le r, \tag{3b}$$

where r is the particle distance, and r_e is the influence radius.

The following equations are the particle interaction models used to discretize the terms in the governing equations.

$$\langle \nabla P \rangle_i = \frac{D}{n^0} \sum_{j \neq i} \frac{P_j + P_i}{|\boldsymbol{r}_j - \boldsymbol{r}_i|^2} (\boldsymbol{r}_j - \boldsymbol{r}_i) W(|\boldsymbol{r}_j - \boldsymbol{r}_i|), \tag{4}$$

$$\langle \nabla \cdot \boldsymbol{V} \rangle_i = \frac{D}{n^0} \sum_{j \neq i} \frac{(\boldsymbol{V}_j - \boldsymbol{V}_i) \cdot (\boldsymbol{r}_j - \boldsymbol{r}_i)}{|\boldsymbol{r}_j - \boldsymbol{r}_i|^2} W(|\boldsymbol{r}_j - \boldsymbol{r}_i|), \tag{5}$$

$$\langle \nabla^2 \phi \rangle_i = \frac{2D}{n^0 \lambda} \sum_{j \neq i} (\phi_j - \phi_i) W(|\boldsymbol{r}_j - \boldsymbol{r}_i|), \tag{6}$$

$$\lambda = \frac{\sum_{j \neq i} W(|\boldsymbol{r}_j - \boldsymbol{r}_i|) |\boldsymbol{r}_j - \boldsymbol{r}_i|^2}{\sum_{j \neq i} W(|\boldsymbol{r}_j - \boldsymbol{r}_i|)}, \tag{7}$$

$$\langle n \rangle_i = \sum_{j \neq i} W(|\boldsymbol{r}_j - \boldsymbol{r}_i|), \tag{8}$$

where D is the number of dimensions, $\boldsymbol{r}$ is the position vector and n^0 is the particle number density at the initial time, and the particle number density is defined as shown in Eq. (8).

2.2. *Pressure Poisson equation*

In this paper, the pressure is calculated by solving the mixed source term Pressure Poisson Equation (PPE) proposed by Tanaka and Masunaga [2010], Lee *et al.* [2011], which can be written as the following equation.

$$\langle \nabla^2 p^{k+1} \rangle_i = (1 - \gamma) \frac{\rho}{\Delta t} \nabla \cdot \boldsymbol{V}_i^* - \gamma \frac{\rho}{\Delta t^2} \frac{\langle n^k \rangle_i - n^0}{n^0}, \tag{9}$$

where p^{k+1}, $\triangle t$, and $\boldsymbol{V}_i^*$ are the pressure of the step $k+1$, time step and temporal velocity and γ is the weight of the particle number density term between 0 and 1 and its value is set to 0.01 in this paper.

2.2.1. *Free surface detection*

The particle number density is used to determine whether a particle is a free surface particle. If $\langle n \rangle_i / n^0 < 0.80$, the particle will be determined as a free surface particle.

If $\langle n\rangle_i/n^0 > 0.97$, the particle will be regarded as an internal fluid particle. If $0.80 < \langle n\rangle_i/n^0 < 0.97$, an additional function needs to be introduced.

$$\langle \boldsymbol{F}\rangle_i = \frac{D}{n^0}\frac{(\boldsymbol{r}_i - \boldsymbol{r}_j)}{|\boldsymbol{r}_i - \boldsymbol{r}_j|}\sum_{j\neq i} W(|\boldsymbol{r}_i - \boldsymbol{r}_j|), \tag{10}$$

where $\langle \boldsymbol{F}\rangle_i$ can be regarded as the asymmetric arrangements of neighbor particles. $|\boldsymbol{F}|^0$ is the initial value of $|\boldsymbol{F}|$ for surface particles. If $\langle|\boldsymbol{F}|\rangle_i > 0.9|\boldsymbol{F}|^0$, the particle will be regarded as a free surface particle.

2.2.2. *Boundary condition*

The multilayer particles' boundary condition is applied to fulfill the support region of the particles near the boundary, as shown in Fig. 1. The pressure of the wall particle is calculated by solving the PPE equation, and ghost particle pressure is obtained by interpolation.

2.3. *Free surface boundary condition*

Virtual particles are arranged over the free surface to fulfill the support domain of the free surface particle, as shown in Fig. 2. The particle number density and the

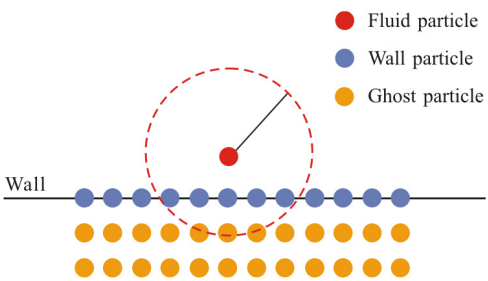

Fig. 1. Schematic of boundary particles.

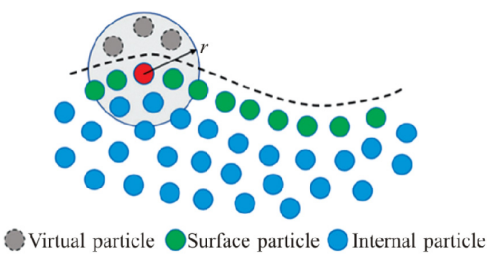

Fig. 2. Schematic of free surface boundary condition.

pressure Laplacian model are modified as

$$\langle n \rangle = \sum_{j \neq i} W_{ji} + \sum_{\text{virtual}} W_{\text{virtual},i} = + \sum_{\text{virtual}} W_{\text{virtual},i}, \tag{11}$$

$$\left\langle \nabla^2 p^{k+1} \right\rangle_i = \frac{2D}{n^0 \lambda} \sum_{j \neq i} (p_j - p_i) W_{ji} + \frac{2D}{n^0 \lambda} \sum_{\text{virtual}} (p_{\text{virtual}} - p_i) W_{\text{virinal},i}, \tag{12}$$

where n_i^* and $W_{\text{virtual},i}$ denote the particle number density of actual neighboring particles and virtual neighboring particles separately.

2.4. *Surface tension model*

The surface tension is imposed by adding a source term to the governing equations, which is proposed by Brackbill *et al.* [1992], as the following equations show:

$$\rho \frac{\mathrm{D}\boldsymbol{V}}{\mathrm{D}t} = -\nabla p + \mu \nabla^2 \boldsymbol{V} + \boldsymbol{F}^V + \boldsymbol{F}^s, \tag{13}$$

$$\boldsymbol{F}^s = \sigma_K \nabla C, \tag{14}$$

where σ is the surface tension coefficient, κ is interface curvature and C is function to mark the free surface particles. For free surface particles $C = 1$, and for internal particles $C = 0$.

3. Numerical Simulation

In this paper, the free damping liquid sloshing phenomena inside a spherical tank with different water depths are simulated. The diameter of the tank is $R = 2\,\mathrm{m}$, and six liquid depths are set up with $h/R = 0.2$, 0.4, 0.8, 1.2, 1.6, 1.8, respectively. The initial particle spacing is $\Delta x = 0.008\ m = 1/250\,\mathrm{R}$, and the time step is $\Delta t = 0.0008\,\mathrm{s}$. The total number of particles corresponding to the six water depths is 181,877, 254,541, 516,971, 665,064, 919,709, and 104,0385, respectively.

The liquid inside the tank is stationary at the starting moment. So, the transverse oscillation motion is applied to the tank as initial excitation. The transverse oscillation frequency is 3.14 rad/s, and the duration is 2 s. After the initial excitation, the liquid sloshing inside the tank decays freely. During the simulation, the center-of-mass coordinates of the liquid in the x, y, and z directions are recorded. And we pay attention to the deformation of the free surface. The frequency of the sloshing can be calculated from the time history curve. And the damping coefficient is calculated by the following equation:

$$\xi = \frac{\ln(x_n/x_m)}{2\pi m}, \tag{15}$$

where ξ represents the damping coefficient of the oscillating liquid sloshing system. x_n is the amplitude of the nth oscillation cycle, and x_m is the amplitude of the mth oscillation cycle of the liquid sloshing. m represents the number of oscillation cycles between the nth and mth cycles.

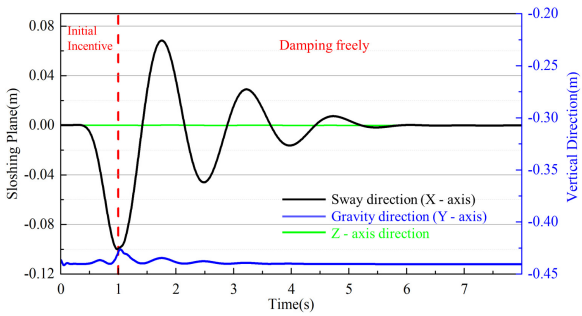

Fig. 3. The mass center coordinates with $h/R = 0.2$.

The numerical simulation in this paper is done by our in-house meshless particle method solver MLParticle-SJTU. This solver has been used to simulate the liquid sloshing problems inside different shapes of liquid tanks many times. For example, Chen and Wan [2019b] simulated the sloshing phenomena inside a rectangular tank and a liquefied natural gas (LNG) tank. Zhang *et al.* [2022a] simulated Faraday waves inside a rectangular cabin with heave motion. Huang *et al.* [2023] simulated Faraday waves inside a cylindrical cabin and a hexagonal prism cabin with heave motion. In these previous papers, the simulation results are in good agreement with the published results obtained by other numerical methods in other groups, which can verify the correctness and effectiveness of the solver used in this paper. Therefore, the correctness of the solver will not be verified again in this paper.

Figure 3 shows the time-history curves of the coordinates of the mass center when the water depth is $h/R = 0.2$. Because, in the case of a low filling rate, less energy is required for full excitation. However, in the case of a high filling rate, more energy is needed for full excitation. Therefore, the excitation time is only 1 s for this working condition, while it is 2 s for other working conditions. In the figure, the black line represents the sway direction (x-axis), the blue line represents the direction of gravity (y-axis), and the green line represents the z-axis direction. As can be seen from the curves, the time-history curve of the coordinate perpendicular to the paper is always approximately zero, indicating that the liquid center of mass nearly has no displacement in this direction and shows a good symmetry of the sloshing. In the gravity direction, the coordinate curve also shows only small fluctuations. The sloshing phenomenon of the liquid is mainly shown in the tank movement direction. From Fig. 3, it can be seen that after the initial excitation lasting for 1s, the liquid sloshing shows a free decay state, with the peak value gradually decreasing, which agrees well with the characteristics of the free decay motion. Through the calculation of this curve, it can be obtained that the intrinsic frequency of the liquid oscillation is about 4.1688 rad/s at this water depth, and the damping ratio is about 0.3997. Figure 4 shows the distribution of the liquid and the pressure distribution. It can be seen from the figure that the fluid pressure distribution is relatively uniform, which

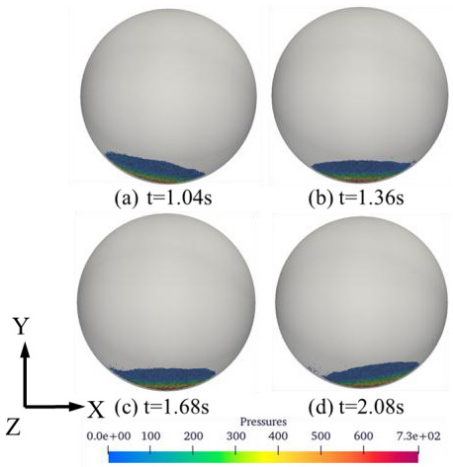

Fig. 4. Liquid distribution of the liquid inside the tank at different times with $h/R = 0.2$.

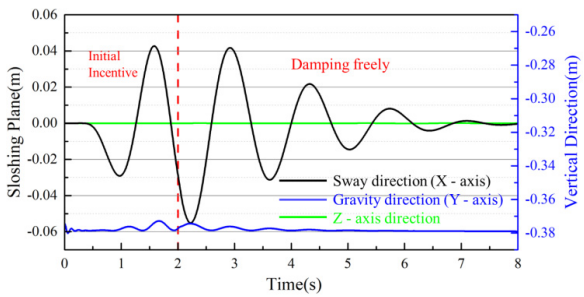

Fig. 5. The mass center coordinates with $h/R = 0.4$.

verifies the stability of the solver in solving the problem. And it can be seen from the figure that at this water depth, the sloshing phenomenon in the liquid tank is not violent, and the shape of the free surface is kept well with no surface curling and breaking.

Figure 5 shows the time history curve of the coordinates of the mass center when the water depth is $h/R = 0.4$. It can be seen from this graph that the characteristics of the curve are basically the same as the case with water depth $h/R = 0.2$. The liquid sloshing is mainly manifested in the direction along the tank movement, and the movement along the other two directions is very small. Through the calculation of the curve, it can be obtained that at this depth, the frequency of free attenuation is 4.3975 rad/s, and the damping ratio is 0.2267. Figure 6 represents the pressure distribution of the liquid at this depth. It can be seen from the figure that the liquid sloshing phenomenon also presents a relatively smooth state at this water depth, and there is no surface curling or breaking.

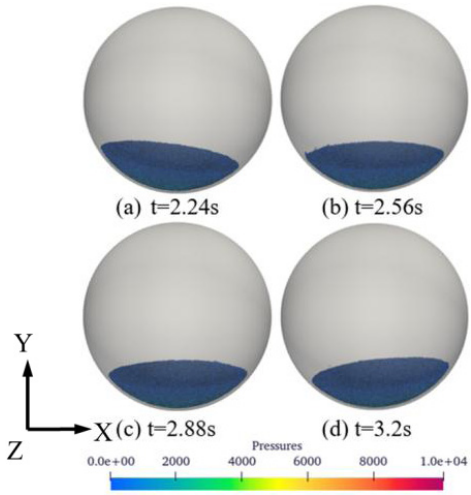

Fig. 6. Liquid distribution of the liquid inside the tank at different times with $h/R = 0.4$.

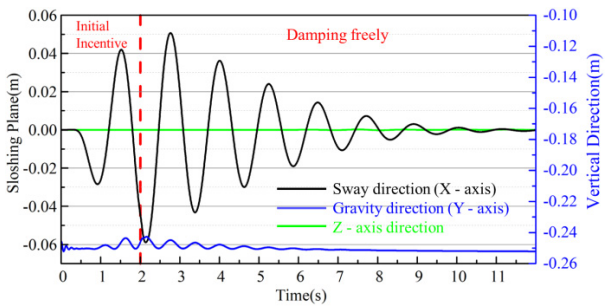

Fig. 7. The mass center coordinates with $h/R = 0.8$.

Figure 7 shows the time history curve of the coordinate when the water depth is $h/R = 0.8$. It can be calculated that the frequency of sloshing at this depth is 5.1206 rad/s, and the damping ratio is 0.0986. Figure 8 represents the pressure distribution of the liquid at this depth. It can be seen that the liquid sloshing phenomenon also presents a relatively stable state at this water depth. Figure 9 shows the time history curve of the coordinates when the water depth is $h/R = 1.2$. It can be obtained that the frequency of free attenuation at this depth is 5.776 rad/s, and the damping ratio is 0.0799. Figure 10 represents the pressure distribution of the liquid at this depth. It can be seen that at this water depth, the sloshing phenomenon of the liquid becomes more intense than before. At this depth, the liquid in the tank climbs upward along the spherical bulkhead during the sloshing, which firstly forms a curling phenomenon, and then the wave surface breaks up, and some droplet splashing phenomena appear in the liquid chamber.

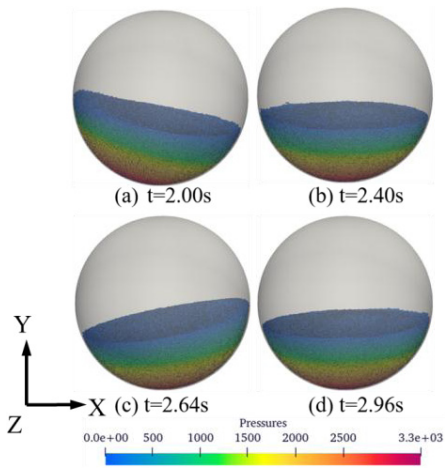

Fig. 8. Liquid distribution of the liquid inside the tank at different times with $h/R = 0.8$.

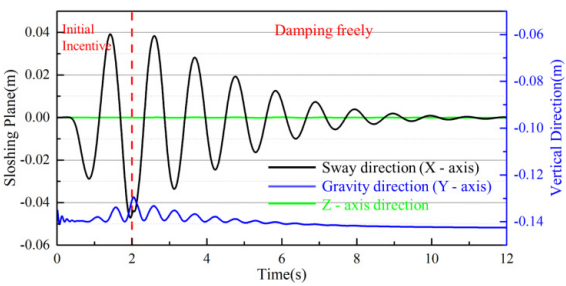

Fig. 9. The mass center coordinates with $h/R = 1.2$.

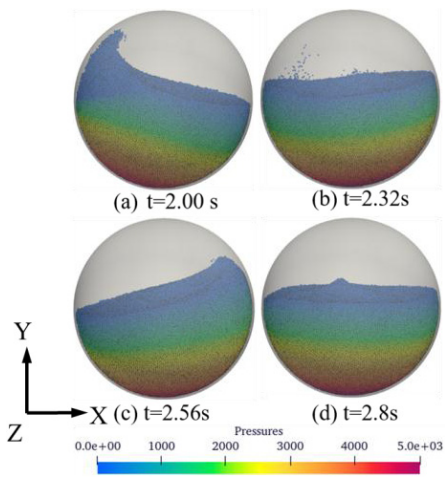

Fig. 10. Liquid distribution of the liquid inside the tank at different times with $h/R = 1.2$.

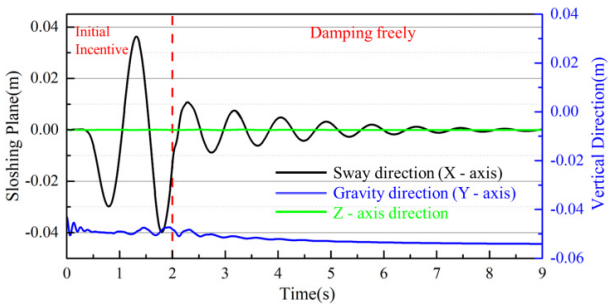

Fig. 11. The mass center coordinates with $h/R = 1.6$.

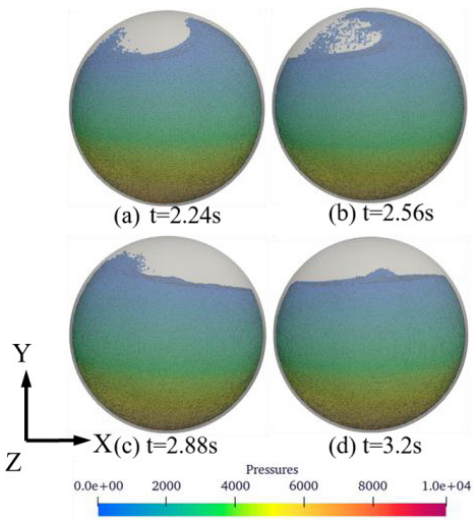

Fig. 12. Liquid distribution of the liquid inside the tank at different times with $h/R = 1.6$.

Figures 11 and 13 represent the time history curves of the liquid center when the water depth is $h/R = 1.6$ and $h/R = 1.8$. As can be seen from the figures, the sloshing amplitudes of these two cases are much smaller compared to the previous cases. In the first 2 s, the large amplitude indicates that the liquid inside the tank is moving together with the tank. When the initial excitation stops, the amplitude of the liquid center of mass curve decreases significantly, indicating that the motion of the liquid center of mass with respect to the tank has been relatively small. It can be seen that the higher filling rate of the liquid chamber can well inhibit the sloshing phenomenon. For the case with $h/R = 1.6$, the sloshing frequency is 7.3513 rad/s, and the damping ratio is 0.0753. For the case with $h/R = 1.8$, the sloshing frequency is 8.3331 rad/s, and the damping ratio is 0.0541. Figures 12 and 14 represent the pressure distribution of the liquid for the two cases $h/R = 1.6$ and $h/R = 1.8$,

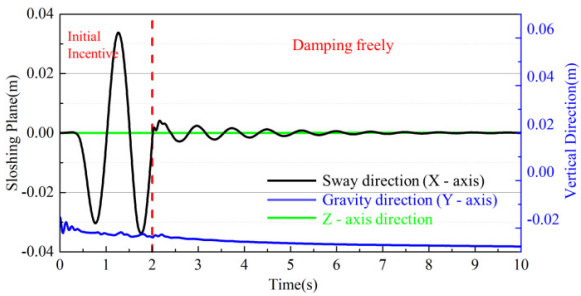

Fig. 13. The mass center coordinates with $h/R = 1.8$.

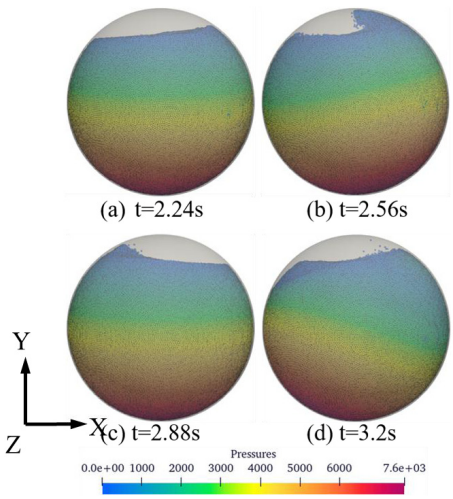

Fig. 14. Liquid distribution of the liquid inside the tank at different times with $h/R = 1.8$.

respectively. It can be seen from the figures that at both sets of depths, an obvious liquid surface curling and breaking occurs, which may be because the angle between the free surface and the bulkhead at this depth is too small, hindering the movement of the liquid climbing upwards along the bulkhead.

In order to further analyze the effect of the water depth on the frequency and the damping coefficient, the frequency and the damping coefficient of the sloshing at different water depths are plotted in a graph for comparison, as shown in Fig. 15. It can be seen that with water depth increasing, the frequency of the liquid sloshing increases, while the damping ratio of the decreases gradually. It can be assumed that increasing water depth brings increasing mass and increasing intrinsic frequency, which are in line with the basic theory in vibration mechanics. The increase in water depth and the decrease in damping coefficient may be due to the fact that the relative motion between the water and the bulkhead is reduced after the water depth is increased, which slows down the damping process of the liquid sloshing.

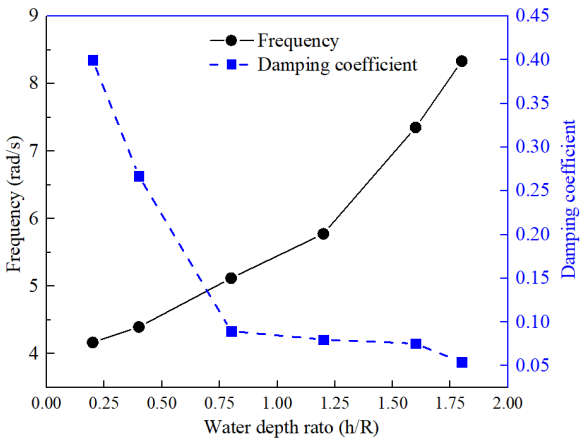

Fig. 15. Comparisons of frequency and damping coefficient at different depths.

4. Conclusions

In this paper, the freely damping sloshing inside a spherical tank is simulated at six different water depths. The nature frequency and the damping coefficients are calculated by the mass center coordinates curves. By comparing the obtained results, it can be found that with the increase of the water depth, the natural frequency of the system gradually increases, while the damping coefficient gradually decreases. Under the same initial excitation, different water depths correspond to different intensities of liquid sloshing. In this paper, for the three cases with $h/R > 1$, the free surface is curled and broken. In contrast, for the three cases with $h/R < 1$, the shape of the free liquid surface remains relatively smooth and stable. This may be due to the fact that when $h/R > 1$, the angle between the free liquid surface and the bulkhead is less than 90°, and the liquid surface curls and breaks under the combined effect of bulkhead pressure and gravity. In the future, the liquid sloshing phenomenon inside the spherical liquid chamber under forced vibration will be further simulated, and the pressure on the bulkhead will be calculated.

Acknowledgment

The authors are grateful for the support from the National Natural Science Foundation of China (52131102).

ORCID

Guohua Pan https://orcid.org/0000-0003-0309-8413
Congyi Huang https://orcid.org/0009-0008-0527-0436
Fengze Xie https://orcid.org/0000-0001-9452-1058
Decheng Wan https://orcid.org/0000-0002-1279-3891

References

Álvaro, R. *et al.* [2021] "Axisymmetric ferrofluid oscillations in a cylindrical tank in microgravity," *Microgravity Sci. Technol.* **33**(4), 1–14.

Brackbill, J. U., Kothe, D. B. and Zemach, C. [1992] "A continuum method for modeling surface tension," *J. Comput. Phys.* **100**(2), 335–354.

Cao, X., Tao, L., Zhang, A. and Ming, F. [2019] "Smoothed particle hydrodynamics (SPH) model for coupled analysis of a damaged ship with internal sloshing in beam seas," *Phys. Fluids* **31**(3), 032103.

Chen, S. *et al.* [2022] "Profiles of liquid on the surface of revolution with varying cross-section under microgravity," *Microgravity Sci. Technol.* **34**(6), 106.

Chen, X. and Wan, D. [2019a] "GPU accelerated MPS method for large-scale 3D violent free surface flows," *Ocean Eng.* **171**, 677–694.

Chen, X. and Wan, D. [2019b] "Numerical simulation of liquid sloshing in LNG tank using GPU-accelerated MPS method," *Chin. J. Theor. Appl. Mech.* **51**(3), 714–729.

Gabriele, B. and Jose, L. [2018] "Co-simulation of ship motions and sloshing in tanks," *Ocean Eng.* **152**(2), 353–376.

Huang, C., Zhang, G., Zhao, W. and Wan, D. [2022] "Hydroelastic responses of an elastic cylinder impacting on the free surface by MPS-FEM coupled method," *Acta Mech. Sin.* **38**(11), 322057.

Huang, C., Zhao, W. and Wan, D. [2023] "Numerical simulations of faraday waves in cylindrical and hexagonal tanks based on MPS method," *J. Hydrodyn.* **35**(2), 93–103.

Lee, B., Park, J., Kim, M. and Hwang, S. [2011] "Step-by-step improvement of MPS method in simulating violent free-surface motions and impact-loads," *Comput. Methods Appl. Mech. Eng.* **200**(9–12), 1113–1125.

Mashy, G. *et al.* [2021] "Smooth particle hydrodynamics simulations of long-duration violent three-dimensional sloshing in tanks," *Ocean Eng.* **229**, 108925.

Tanaka, M. and Masunaga, T. [2010] "Stabilization and smoothing of pressure in MPS method by quasi-compressibility," *J. Comput. Phys.* **229**(11), 4279–4290.

Tang, Z., Zhang, Y. and Wan, D. [2016] "Multi-resolution MPS method for free surface flows," *Int. J. Comput. Methods* **13**(4), 1641018.

Wang, L., Zhang, X., Yun, Y., Liu, J., Li, W. and Huang, B. [2022] "Numerical simulation of reorientation process under different conditions in a vanetype surface tension propellant tank," *Microgravity Sci. Technol.* **34**, 37.

Xie, F., Meng, Q. and Wan, D. [2022] "Numerical simulations of liquid-solid flows in a vertical pipe by MPS−DEM coupling method," *China Ocean Eng.* **36**, 542–552.

Xie, F., Pan, G., Zhao, W. and Wan, D. [2025] "Unresolved MPS-DEM coupling method for three-dimensional liquid-solid dam-break flows impacting on rigid structures," *Ocean Eng.* **323**, 120601.

Xie, F., Zhao, W. and Wan, D. [2021] "MPS-DEM coupling method for interaction between fluid and thin elastic structures," *Ocean Eng.* **236**, 109449.

Yang, H. Q. and Peupeot, J. [2014] "Propellant sloshing parameter extraction from computational-fluid-dynamics analysis," *J. Spacecr. Rockets* **51**(3), 908–916.

Yang, X. *et al.* [2022] "Simulating multi-phase sloshing flows with the SPH method," *Appl. Ocean Res.* **118**, 102989.

Zhang, G., Zha, R. and Wan, D. [2022a] "MPS-FEM coupled method for 3D dam-break flows with elastic gate structures," *Eur. J. Mech. B: Fluids* **94**, 171–189.

Zhang, G., Zhao, W. and Wan, D. [2022b] "Numerical simulations of sloshing waves in vertically excited square tank by Improved MPS method," *J. Hydrodyn.* **34**(1), 76–84.
Zhang, Y. [2014] Development and application of 3D parallel improved meshless MPS method, PhD Thesis, Shanghai Jiao Tong University, China.
Zhang, Y. and Wan, D. [2014] "Comparative study of MPS method and level-set method for sloshing flows," *J. Hydrodyn.* **26**(4), 577–585.